GPS Solutions (2019) 23:18
https://doi.org/10.1007/s10291-018-0810-2

ORIGINAL ARTICLE

Single-frequency precise point positioning (PPP) for retrieving ionospheric TEC from BDS B1 data

Min Li[1] · **Baocheng Zhang**[1] · **Yunbin Yuan**[1] · **Chuanbao Zhao**[1,2]

Received: 9 May 2018 / Accepted: 1 December 2018 / Published online: 13 December 2018

Abstract

The customary approach to determine ionospheric total electron content (TEC) with BeiDou navigations satellite system (BDS) data normally requires dual-frequency (DF) data provided by geodetic-grade receivers. In this study, we present an analysis of the performance of a new TEC estimation procedure based on single-frequency (SF) BDS data. First, the ionospheric observable is retrieved from the SF BDS code and phase data using precise point positioning (PPP) instead of the carrier-to-code leveling (CCL) technique used in the customary DF method. Then, the absolute ionospheric slant TEC (STEC) values are isolated from the ionospheric observables by modeling the ionospheric observable with the adjusted spherical harmonic (ASH) expansion and constraining the satellite differential code bias (SDCB) to very precise values provided externally. The experimental data were taken from the multi-GNSS experiment (MGEX) network for high and low sunspot periods, covering the 2 months, i.e., December 2014 and September 2017. The TEC data obtained from the combined final global ionospheric map (GIM) provided by the international GNSS service (IGS), the JASON DF altimeter, and the BDS-measured differential STEC (dSTEC) are used as reference data to evaluate the performance of the TEC values estimated by the proposed method. The evaluation results indicate that compared to the reference TEC data, the ionospheric TEC estimated by the proposed method using BDS B1 data and the customary CCL-based DF method based on BDS B1 + B2 data, perform at roughly equal levels.

Keywords BeiDou navigation satellite system (BDS) · Single frequency (SF) · Total electron content (TEC) · Precise point positioning (PPP) · Satellite differential code biases (SDCBs) · Carrier-to-code leveling (CCL)

Introduction

Taking advantage of the dispersive nature of the ionospheric refractivity, global navigation satellite system (GNSS) can make remarkable contributions to monitoring spatial and temporal structure and variability of the ionosphere by measuring the total electron content (TEC) of the ionosphere (Brunini et al. 2005). On the other hand, it is well-known that ionospheric delay accounts for one of the largest and most variable sources of error in GNSS applications (Feltens and Schaer 1998; Krankowski et al. 2005). For the single-frequency (SF) GNSS receivers, one important way to mitigate the ionospheric error is to introduce external ionospheric TEC information or models (Wang et al. 2016a; Li et al. 2018a). Therefore, GNSS retrieval of ionospheric TEC is and remains to be an important issue in the precise positioning and timing of applications (Mannucci et al. 1998; Hernandez-Pajares et al. 1999).

Following the success of the GPS and the GLONASS system, the Chinese BeiDou navigations satellite system (BDS) began providing continuous positioning, navigation and timing services in the Asia-Pacific area at the end of 2012 (Montenbruck and Steigenberger 2013). By the end of 2016, the regional BDS (BDS-2) comprised a total of 6 geostationary orbit (GEO) satellites, 6 inclined geosynchronous orbit (IGSO) satellites and 4 medium earth orbit (MEO) satellites. On March 30, 2015, China began to build the 3rd generation BeiDou system (BDS-3), which will offer a fully global navigation service by 2020. At the end of August 2018, seventeen BDS-3 in-orbit validation satellites had been launched (http://mgex.igs.org/IGS_MGEX_Statu

✉ Baocheng Zhang
b.zhang@whigg.ac.cn

[1] State Key Laboratory of Geodesy and Earth's Dynamics, Institute of Geodesy and Geophysics, Wuhan, China

[2] University of Chinese Academy of Sciences, Beijing, China

s_BDS.php). The multi-GNSS experiment (MGEX) project undertaken by the international GNSS service (IGS) provides an excellent opportunity to track all available GNSS signals and to conduct tracking data analysis (Montenbruck et al. 2014). The MGEX network and the signals transmitted by the current BDS satellites make it possible to apply multi-constellation and multi-frequency observations to precise ionospheric TEC estimation.

Over decades, considerable effort has been put into developing methods for GNSS-based ionosphere TEC retrieval (Komjathy et al. 2005). The commonly used ionospheric TEC determination methods can be classified into two main categories: (1) the dual-frequency (DF) approach and (2) the SF approach.

As one of the simplest and effective DF methods, the carrier-to-code leveling (CCL) method has been widely used for retrieving ionospheric observables based on geometry-free (GF) linear combinations of GNSS pseudorange and carrier phase measurements (Hernandez-Pajares et al. 2011; Zhang 2016). The ionospheric observables obtained from the CCL technique can be interpreted as a combination of the slant TEC (STEC) along the satellite-receiver line-of-sight, the satellite differential code biases (SDCBs), and the receiver DCBs (Li et al. 2017a). According to the study of Ciraolo et al. (2007), there is a systematic arc-dependent error called leveling error which is induced by code-delay noise and multi-path effects in the CCL-based ionospheric observable (Brunini and Azpilicueta 2009). With the goal of attaining more accurate TEC measurement retrieval, Zhang et al. (2012) proposed a DF method for extracting ionospheric observables from raw observations using precise point positioning (PPP). Considering that the PPP-derived ionospheric observables have an identical form to their counterparts obtained from leveling the GF GNSS carrier phase to code but are less affected by the extracting error, this PPP-based method has also been widely used in GNSS-based ionospheric studies (Yuan et al. 2015; Liu et al. 2016).

Compared with the more common DF approach, an attractive advantage of the SF method is that it can work with mass-market SF receivers, which are much more cost-effective than geodetic-grade DF receivers. Several studies have already been performed regarding SF GNSS retrieval of TEC (Yuan and Ou 2001; Wu et al. 2006; Schueler and Oladipo 2013), and most of the literature focuses on the code-minus-carrier (CMC) combination method. Schueler and Oladipo (2014) found that the CMC-based SF method is suitable for ionosphere monitoring for mid- and high-latitude sites; however, the precision level of CMC-based TEC estimate is bounded by the code-delay noise and multi-path effects. Zhang et al. (2017) proposed a SF PPP approach that enables the joint estimation of vertical TEC (VTEC) and SDCBs, and found that the SF approach performs well when applied to GPS L1 data collected by a single receiver. However, only GPS was considered in their study. Compared to other GNSS systems, BDS is the only navigation system employing GEO, IGSO, MEO satellites in a common constellation. According to the studies of Shu et al. (2016) and Wang et al. (2016b), both the precision and stability of BDS SDCB, estimated together with ionospheric model coefficients from BDS data, are lower compared with those of GPS and Galileo. The reasons of this phenomenon are related to the sparsely distributed tracking stations of BDS and the quality of BDS observables. Therefore, it is worthwhile to study how to obtain high-precision ionospheric TEC using the BDS data on just one frequency.

The first contribution of this work is thus to modify the methodology presented by Zhang et al. (2017) in such a way that the SDCBs are not estimated together with the ionospheric model coefficients any longer, but fixed them to the very precise values available from externally sources. In addition, when performing the ionospheric TEC accuracy validation in Zhang et al. (2017), there is no other external reference TEC data used except for the customary CCL-based TEC estimates, implying that only intra-technique comparison has been conducted. With this in mind, we consider more studies on the issue of performance analysis of SF-based ionospheric TEC by means of inter-technique comparison, that is, by comparing them with external reference TEC data and using different ionospheric modeling methods. This is the other contribution of the present work.

In this study, we propose a new TEC estimation procedure based on SF BDS data. The next section presents the proposed method to determine ionospheric TEC based on SF BDS data, the following section describes the experimental data and processing strategies. Then we show the preliminary experimental results. In the end, we present conclusions about the results. It should be noted that we hereafter refer to the ionospheric TEC determination approach using the CCL method based on the BDS B1 + B2 data as the DF approach.

Methodology

The SF-based algorithm for estimating the ionospheric TEC is described in detail in this section. Generally, it consists of two sequential steps: first, extract the ionospheric observables from the original SF BDS code and carrier phase observations; second, separate the ionospheric TEC from the ionospheric observables by establishing an ionospheric model and fixing SDCBs to very precise values provided externally.

Extraction of ionospheric observables from SF BDS measurements

The mathematical expression for BDS code and carrier phase, which is observable in units of length, can be expressed as follows (Leick et al. 2015; Li et al. 2017b):

$$\begin{cases} P^s_{r,j}(k) = \rho^s_r(k) + dt_r(k) - dt^s(k) + T^s_r(k) + \mu_j \cdot I^s_{r,1}(k) + b_{r,j} - b^s_j + \varepsilon_p(k) \\ \phi^s_{r,j}(k) = \rho^s_r(k) + dt_r(k) - dt^s(k) + T^s_r(k) - \mu_j \cdot I^s_{r,1}(k) + N^s_{r,j} + \varepsilon_\phi(k) \end{cases} \tag{1}$$

where $P^s_{r,j}(k)$ and $\phi^s_{r,j}(k)$ denote the code and carrier phase observations from satellite s to receiver r on frequency band j at epoch k; $\rho^s_r(k)$ is the geometric vacuum distance from the satellite at the epoch of transmission to reception at the receiver; $dt_r(k)$ and $dt^s(k)$ refer to the receiver and satellite clock errors; $T^s_r(k)$ is the slant tropospheric delay; $I^s_{r,1}$ is the ionospheric delay on the first frequency; $\mu_j = \frac{f_1^2}{f_j^2}$ is the frequency-dependent factor that is used to convert ionospheric delay from the first frequency to other frequencies; $b_{r,j}$ and b^s_j are the receiver and satellite code hardware delays; $N^s_{r,j}$ is the carrier phase ambiguity in length absorbing receiver and satellite phase instrumental delays and initial phase biases; $\varepsilon_{\mathrm{p}}(k)$ and $\varepsilon_\phi(k)$ are the combinations of the observational noise and multipath in code and carrier phase observations.

Generally, the precise satellite clock products provided by IGS are generated using the ionospheric-free (IF) combination. Therefore, the published IGS satellite clock offsets $\mathrm{d}t^s_I$ absorb the IF combination of satellite code hardware delays as follows (Li et al. 2012; Zhang et al. 2017):

$$\mathrm{d}t^s_I(k) = \mathrm{d}t^s(k) + \frac{\mu_2}{\mu_2 - 1} b^s_1 - \frac{1}{\mu_2 - 1} b^s_2 \tag{2}$$

which should be carefully considered when using raw observations since satellite clock offsets are fixed to the precise products in PPP processing. Using the a priori known receiver coordinate and satellite coordinate and considering (2), the code and carrier phase observation equation on the first frequency can be expressed as:

$$\begin{cases} \Delta P^s_{r,1}(k) = P^s_{r,1}(k) - \rho^s_r(k) + \mathrm{d}t^s_I(k) - T^s_{r,0}(k) \\ \qquad = m^s_r(k) \cdot \mathrm{ZTD}_r(k) + \mathrm{d}t_r(k) + b_{r,1} + I^s_{r,1}(k) + \dfrac{1}{\mu_2 - 1}(b^s_1 - b^s_2) + \varepsilon_{\mathrm{p}}(k) \\ \Delta \phi^s_{r,1}(k) = \phi^s_{r,1}(k) - \rho^s_r(k) + \mathrm{d}t^s_I(k) - T^s_{r,0}(k) \\ \qquad = m^s_r(k) \cdot \mathrm{ZTD}_r(k) + \mathrm{d}t_r(k) - I^s_{r,1}(k) + N^s_{r,1} + \dfrac{\mu_2}{\mu_2 - 1} b^s_1 - \dfrac{1}{\mu_2 - 1} b^s_2 + \varepsilon_\phi(k) \end{cases} \tag{3}$$

where $\Delta P^s_{r,1}(k)$ and $\Delta \phi^s_{r,1}(k)$ denote the observed-minus-calculated code and carrier phase observations; $\rho^s_r(k)$ is the geometric distance computed from a priori known receiver coordinate and satellite coordinate; $T^s_{r,0}(k)$ is the approximate slant tropospheric delay computed using an empirical model; $ZTD_r(k)$ is the zenith tropospheric delay at the receiver, and $m^s_r(k)$ is the corresponding mapping function.

Note that (3) represents a rank-deficient system and does not have a unique solution. This issue can be eliminated using a re-parameterization process (Odijk et al. 2016), which is given as follows:

$$\begin{cases} \Delta P^s_{r,1}(k) = m^s_r(k) \cdot \mathrm{ZTD}_r(k) + \left(\mathrm{d}t_r(k) + b_{r,1}\right) \\ \qquad + \left(I^s_{r,1}(k) + \dfrac{1}{\mu_2 - 1}(b^s_1 - b^s_2)\right) + \varepsilon_{\mathrm{p}}(k) \\ \qquad = m^s_r(k) \cdot \mathrm{ZTD}_r(k) + \mathrm{d}\hat{t}_r(k) + \hat{I}^s_{r,1}(k) + \varepsilon_p(k) \\ \Delta \phi^s_{r,1}(k) = m^s_r(k) \cdot \mathrm{ZTD}_r(k) + \left(\mathrm{d}t_r(k) + b_{r,1}\right) \\ \qquad - \left(I^s_{r,1}(k) + \dfrac{1}{\mu_2 - 1}(b^s_1 - b^s_2)\right) \\ \qquad + \left(N^s_{r,1} - b_{r,1} + \dfrac{1}{\mu_2 - 1}(b^s_1 - b^s_2) \right. \\ \qquad \left. + \dfrac{\mu_2}{\mu_2 - 1} b^s_1 - \dfrac{1}{\mu_2 - 1} b^s_2\right) + \varepsilon_\phi(k) \\ \qquad = m^s_r(k) \cdot \mathrm{ZTD}_r(k) + \mathrm{d}\hat{t}_r(k) - \hat{I}^s_{r,1}(k) \\ \qquad + \hat{N}^s_{r,1} + \varepsilon_\phi(k) \end{cases} \tag{4}$$

where identifiers with ∧ on the top denote the re-parameterized parameters of the model,

$$\begin{cases} \widehat{dt}_r(k) = dt_r(k) + b_{r,1} \\ \widehat{I}^s_{r,1}(k) = I^s_{r,1}(k) - \dfrac{1}{\mu_2 - 1} \cdot DCB^s \\ \hat{N}^s_{r,1} = N^s_{r,1} - b_{r,1} + \dfrac{\mu_2 + 1}{\mu_2 - 1} \cdot b^s_1 - \dfrac{2}{\mu_2 - 1} \cdot b^s_2 \end{cases} \tag{5}$$

with $\mathrm{DCB}^s = b_2^s - b_1^s$ being the satellite DCB.

We can find that (4) still has a rank deficiency of one size, the re-parameterized parameters $\mathrm{d}\hat{t}_r(k)$, $\hat{I}^s_{r,1}(k)$ and $\hat{N}^s_{r,1}$ are still not individually estimable. To cope with this problem, we re-parameterize the clock as the changes of the original receiver clocks relative to the first epoch, and estimate such receiver clock offsets re-parameterized as white noise. Consequently, the resulting full-rank observation equations can be expressed as follows:

$$\begin{cases} \Delta P^s_{r,1}(k) = m^s_r(k)\cdot \mathrm{ZTD}_r(k) + \mathrm{d}\bar{t}_r(k) + \bar{I}^s_{r,1}(k) + \varepsilon_{\mathrm{p}}(k) \\ \Delta \phi^s_{r,1}(k) = m^s_r(k)\cdot \mathrm{ZTD}_r(k) + \mathrm{d}\bar{t}_r(k) - \bar{I}^s_{r,1}(k) + \bar{N}^s_{r,1} + \varepsilon_{\phi}(k) \end{cases} \tag{6}$$

where

$$\begin{cases} \mathrm{d}\bar{t}_r(k) = \mathrm{d}\hat{t}_r(k) - \mathrm{d}\hat{t}_r(1) = \mathrm{d}t_r(k) - \mathrm{d}t_r(1) \\ \bar{I}^s_{r,1}(k) = \hat{I}^s_{r,1}(k) + \mathrm{d}\hat{t}_r(1) = I^s_{r,1}(k) - \dfrac{1}{\mu_2 - 1}\cdot \mathrm{DCB}^s + \mathrm{d}\hat{t}_r(1) \\ \bar{N}^s_{r,1} = \hat{N}^s_{r,1} + 2\mathrm{d}\hat{t}_r(1) \end{cases} \tag{7}$$

with $\mathrm{d}\bar{t}_r(k)$, $\bar{I}^s_{r,1}(k)$ and $\bar{N}^s_{r,1}$ being the estimable receiver clocks, ionospheric observables and ambiguities, respectively.

Applying the same deviation process to the second frequency, the full-rank observation equations can be expressed as:

$$\begin{cases} \Delta P^s_{r,2}(k) = m^s_r(k)\cdot \mathrm{ZTD}_r(k) + \mathrm{d}\bar{t}_r(k) + \bar{I}^s_{r,2}(k) + \varepsilon_{\mathrm{p}}(k) \\ \Delta \phi^s_{r,2}(k) = m^s_r(k)\cdot \mathrm{ZTD}_r(k) + \mathrm{d}\bar{t}_r(k) - \bar{I}^s_{r,2}(k) + \bar{N}^s_{r,2} + \varepsilon_{\phi}(k) \end{cases} \tag{8}$$

where

$$\begin{cases} \mathrm{d}\hat{t}_r(1) = \mathrm{d}t_r(1) + b_{r,2} \\ \mathrm{d}\bar{t}_r(k) = \mathrm{d}t_r(k) - \mathrm{d}t_r(1) \\ \bar{I}^s_{r,2}(k) = I^s_{r,2}(k) - \dfrac{\mu_2}{\mu_2 - 1}\cdot \mathrm{DCB}^s + \mathrm{d}\hat{t}_r(1) \\ \bar{N}^s_{r,2} = N^s_{r,2} - b_{r,2} + \dfrac{2\mu_2}{\mu_2 - 1}\cdot b^s_1 - \dfrac{\mu_2 + 1}{\mu_2 - 1}\cdot b^s_2 + 2\mathrm{d}\hat{t}_r(1) \\ \Delta P^s_{r,2}(k) = P^s_{r,2}(k) - \rho^s_r(k) + \mathrm{d}t^s_I(k) - T^s_{r,0}(k) \\ \Delta \phi^s_{r,2}(k) = \phi^s_{r,2}(k) - \rho^s_r(k) + \mathrm{d}t^s_I(k) - T^s_{r,0}(k) \end{cases} \tag{9}$$

with $\bar{I}^s_{r,2}(k)$ and $\bar{N}^s_{r,2}$ being the estimable ionospheric observables and ambiguities on the second frequency, respectively.

Apparently from (7) and (9), the estimable ionospheric observables $\bar{I}^s_{r,1}$ and $\bar{I}^s_{r,2}$ from SF BDS measurements are biased by the SDCB, the combination of the receiver clock at the first epoch and the receiver hardware delay on the corresponding frequency.

Ionospheric TEC modeling

Once the ionospheric observables are obtained, the absolute ionospheric TEC can be isolated from the ionospheric observables in two different ways: (1) the ionospheric model parameters are estimated in conjunction with SDCB parameters and biased receiver clock parameters; and (2) the ionospheric model parameters and biased receiver clock parameters are simultaneously estimated by constraining the SDCB to a priori known values, such as the multi-GNSS DCB products provided by the German aerospace center (DLR) or the Chinese academy of sciences (CAS) (available at: ftp://igs.ign.fr/pub/igs/products/mgex/dcb/) (Li et al. 2018b). In this study, we use the adjusted spherical harmonic (ASH) expansion based on a thin-layer approximation to model variation of ionospheric VTEC (Liu et al. 2018), which reads,

$$\begin{cases} \mathrm{VTEC}(\varphi', \lambda') = \sum\limits_{n=0}^{4}\sum\limits_{m=0}^{n} \tilde{P}_{nm}(\sin\varphi')\cdot\left(\tilde{E}_{nm}\cos(m\lambda') + \tilde{F}_{nm}\sin(m\lambda')\right) \\ \varphi' = \pi/2 - \dfrac{\pi\left(\pi/2 - \cos\varphi_C\right)}{\theta_{\max}} \\ \varphi_C = \arccos[\sin\varphi\sin\varphi_N + cos\varphi cos\varphi_N\cos(\lambda_N - \lambda)] \\ \lambda' = \arcsin(\dfrac{\sin(\lambda - \lambda_N)}{\sin\varphi_C}\cos\varphi) \end{cases} \tag{10}$$

where VTEC is the ionospheric VTEC at the ionospheric intersecting pierce point (IPP); φ and λ are the geomagnetic latitude and longitude of the IPP; φ_N and λ_N are the geomagnetic latitude and longitude of the central point of the selected region; φ' and λ' are the projected latitude and longitude in the sphere cap coordinate system; $\theta_{\max}$ is the half angle of the sphere cap; $\tilde{P}_{nm}(\sin\phi) = N_{nm}\cdot P_{nm}(\sin\phi)$ is the normalized associated Legendre function of degree n and order m; $N_{nm} = \sqrt{\frac{(n-m)!(2n+1)(2-\delta_{0m})}{(n+m)!}}$ is the normalization function and δ is the Kronecker delta; $P_{nm}(\sin\phi)$ is the classical, unnormalized Legendre function; $\tilde{E}_{nm}$ and $\tilde{F}_{nm}$ are the unknown ASH coefficients to be estimated.

The BDS SDCB products for the year of 2017 provided by the DLR and for the year of 2014 provided by the CAS are used to eliminate the impact of SDCB. The biased receiver clock at the first epoch is estimated in conjunction with ionospheric model parameters using the least squares fitting technique. Considering (7), the observation equation can be expressed as follows:

$$\begin{cases} \bar{I}^s_{r,1} - \dfrac{1}{\mu_2 - 1}(\mathrm{DCB}^s) = \dfrac{A}{f_1^2}\cdot \mathrm{MF}(z)\cdot \mathrm{VTEC} + \mathrm{d}\hat{t}_r(1) \\ P = \dfrac{1}{1 + \cos^2 E} \end{cases} \tag{11}$$

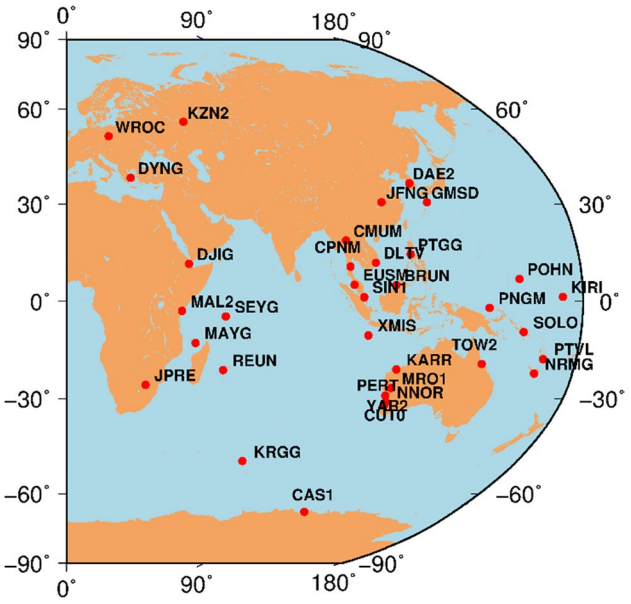

Fig. 1 Distribution of the selected MGEX receivers

where $A = 40.28 \times 10^{16}$; $\mathrm{MF}(z) = [1 - \cos^2 E \cdot R_e^2/(R_e + 450)^2]^{-1/2}$ is the mapping function used to convert the slant to the vertical TEC, denoted by the elevation angle E of the satellite-linked to the corresponding receiver (Schaer 1999; Brunini and Azpilicueta 2010); R_e represents the mean radius of the earth in kilometers; P is the weight of the ionospheric observable depends on the elevation angle of the satellite. To mitigate the impact of multipath and mapping function errors at low elevations, we only use the data with elevation angles above 10° in the process of ionospheric TEC modeling.

Experimental data and processing strategies

As shown in Fig. 1, a set of BDS data collected by 35 MGEX receivers at a 30 s sampling rate were selected to assess the performance of the SF approach. Two test periods consisting of the months of December 2014 and September 2017 were chosen to sample both high and low solar activity conditions. Table 1 shows the models and strategies used in this study when implementing SF PPP to retrieve the ionospheric observables. The data from the selected stations are processed on a day-by-day basis.

Preliminary results and analysis

We evaluate the ionospheric estimation accuracy by analyzing the consistency between the ionospheric TEC estimates, determined using both SF and DF methods, and the external ionospheric products. Three representative assessment methods are applied to the ionospheric TEC accuracy validation: (1) a comparison between the VTEC estimates at IPPs of each BDS receiver with the IGS combined final global ionospheric maps (GIMs); (2) a comparison between the GNSS-based TEC estimates with TEC measurements provided by

Table 1 Models and strategies used in SF PPP

Item	Models/strategies
Observations	BDS raw code and phase observations
Estimator	Kalman filter
Frequency selection	B1
Sampling rate	30 s
Elevation cutoff angle	10°
Weighing strategy	A-priori precision of 0.003 and 0.3 m for raw phase and code; Elevation-dependent weighing ($P = \sin^2(E)$) is used
Satellite phase center	Phase center offsets and variation values for BDS corrections from Wuhan University (Guo et al. 2016) are used
Receiver phase center	Phase center offsets and variation values for BDS are assumed the same with for GPS corrections from igs08.atx
Phase windup	Corrected
Tidal effects tides	Consider solid tides, ocean loading and polar tides
Satellite orbit and clock	Fixed to the IGS MGEX (GBM) final products
Receiver clock offset	Estimated as white noise
Station coordinates	IGS weekly combination
Zenith tropospheric delay	A priori value provided by the Saastamoinen model; estimated as random-walk noise (10^{-7} m^2/s); GMF is used
Slant ionospheric delay	Estimated as white noise
Phase ambiguities	Estimated as float constants for each arc

DF JASON altimeters; and (3) a comparison between the variations of STEC estimates with the observed STEC variations along a phase-continuous transmitter–receiver arc collected from BDS receivers. The customary DF CCL method is also used as a reference to validate the performance of the SF-based TEC. It should be noted that the SF data tested in this study were collected from geodetic-grade receivers, the performance of TEC estimated by SF data with low-cost receivers connected to patch-type antennas will be discussed in the future work.

Validation against GIM TEC

The IGS combined final GIM product, which has been acknowledged as one of the most accurate post-processed TEC products with an accuracy of 2–8 TEC units (TECU, 10^{16} electrons/m^2) (see http://www.igs.org/products) (Hernández-Pajares et al. 2009), is used as a reference in the performance assessment of the SF ionospheric TEC determination method.

Taking stations JFNG and XMIS as an example, we plot in Figs. 2 and 3 the daily time series of absolute VTEC values determined using, respectively, the SF approach based on the BDS B1 data, the DF method based on the BDS B1 + B2 data, and the IGS GIM for IPPs. JFNG is located at mid-latitudes in the northern hemisphere and XMIS is located at low latitudes in the southern hemisphere. The period consists of day of year (DOY) 349–355 in 2014 and 262–268 in 2017. Compared to Fig. 3, Fig. 2 shows a significant decrease in the TEC values in response to the decline

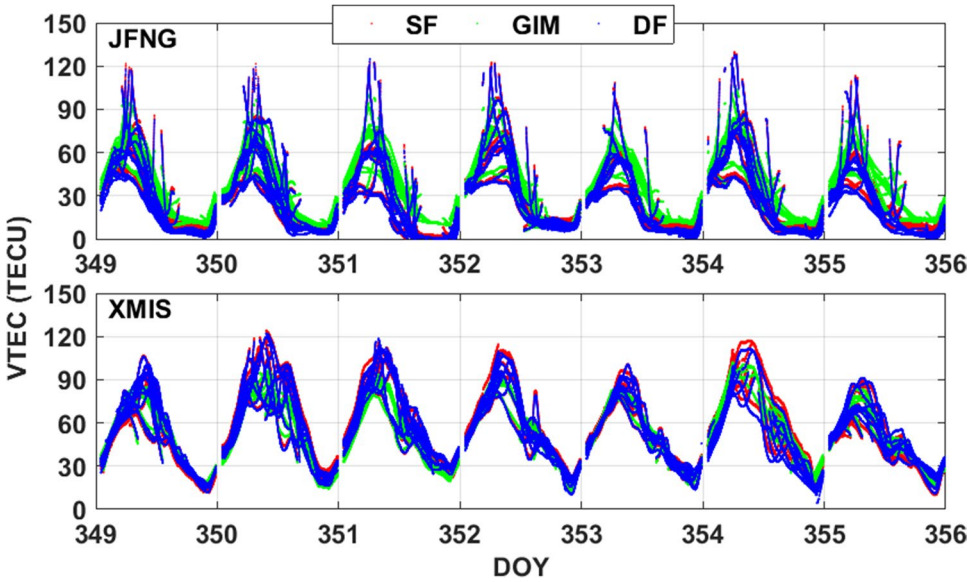

Fig. 2 Daily time series of VTEC values estimated from BDS B1 + B2 data (in blue), from BDS B1 data (in red), and IGS GIM data (in green) at the sites JFNG and XMIS for the period DOY 349–355 in 2014

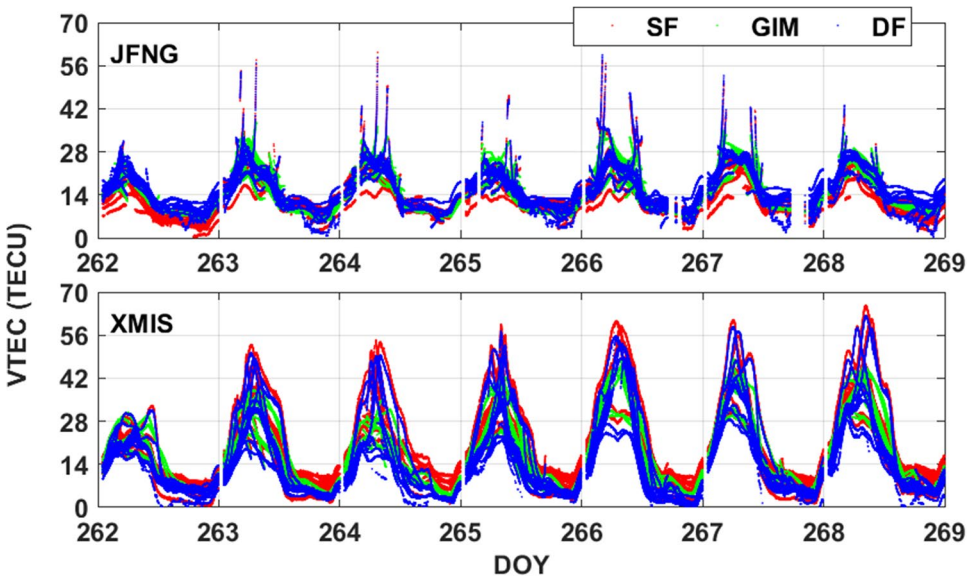

Fig. 3 Daily time series of VTEC values estimated from BDS B1 + B2 data (in blue), from BDS B1 data (in red), and IGS GIM data (in green) at the sites JFNG and XMIS for the period DOY 262–268 in 2017

of the solar activity level. It is apparent that the time series of VTEC estimates determined by the SF approach and DF method have a similar trend with the GIM TEC, they can all represent the diurnal variation of the ionosphere during both high and low solar activity periods.

To further quantify the consistency among the time series of VTEC estimates listed in each panel of Figs. 2 and 3, using the GIM TEC values as a reference, the mean bias and the root mean square (RMS) error of the VTEC estimates determined by the SF and DF methods are presented in Figs. 4 and 5. For the high solar activity year, the mean RMS value of the differences between the VTEC derived from the SF/DF model and GIM are approximately 8.01/10.25 and 7.05/7.22 TECU for the stations JFNG and XMIS, respectively. For the low solar activity year, the mean RMS value of the differences of the VTEC derived from the SF/DF model with respect to GIM-based TEC are approximately 2.66/2.68 and 4.11/3.44 TECU for the stations JFNG and XMIS, respectively.

Concerning the statistical results for all selected stations summarized in Table 2, the VTEC time series estimated by the SF method agrees better with the IGS GIM products than those estimated by the DF method for the high solar activity period. For the low solar activity period, the TEC estimated by the DF method agrees better with the IGS GIM product than those estimated by the SF method.

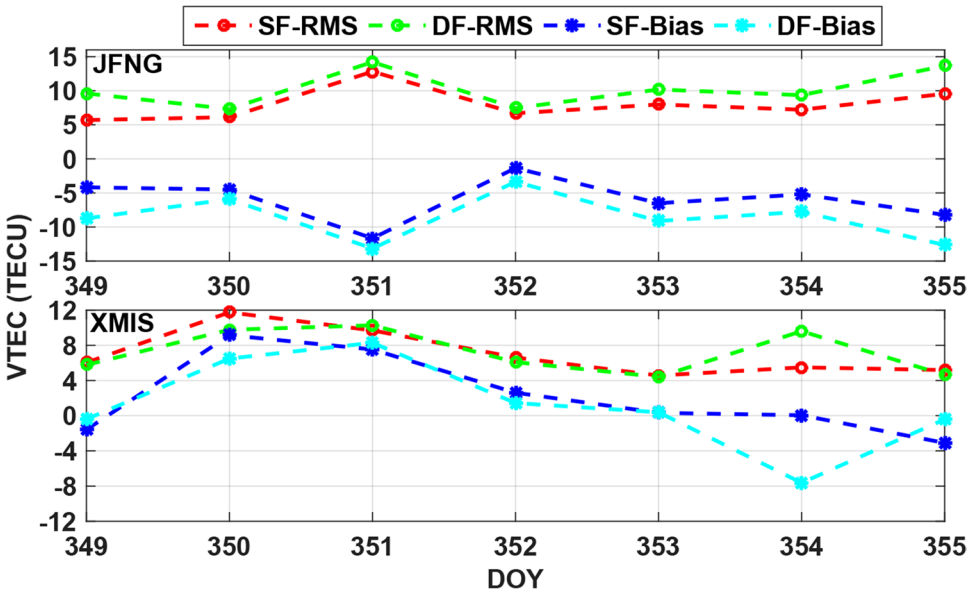

Fig. 4 Daily mean and RMS of the differences between the VTEC estimates relative to GIM at the sites JFNG and XMIS for the period DOY 349–355 in 2014 (unit: TECU)

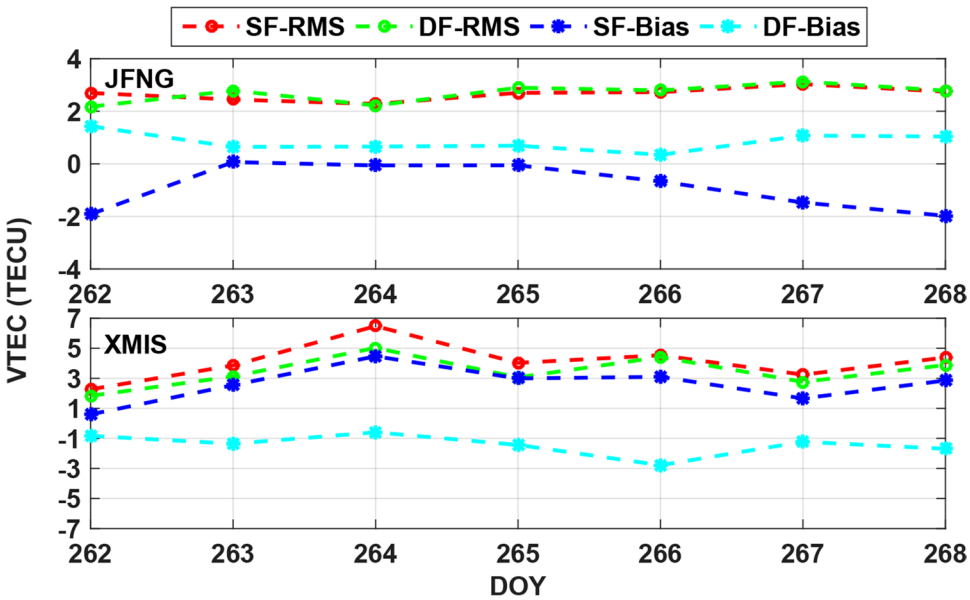

Fig. 5 Daily mean and RMS of the differences between the VTEC estimates relative to GIM at the sites JFNG and XMIS for the period DOY 262–268 in 2017 (unit: TECU)

Table 2 Monthly mean and RMS of the differences between the VTEC estimates relative to GIM TEC for all selected receivers (unit: TECU)

Period	Month	SF RMS	DF RMS	SF mean bias	DF mean bias
High solar activity 2014	12	5.77	6.80	− 0.56	− 3.72
Low solar activity 2017	9	3.65	2.48	− 0.23	− 0.55

Validation against JASON TEC

The DF ocean altimeter on board the JASON satellite can provide a measurement of the VTEC over its footprint (Orus et al. 2007), with a systematic bias of approximately 2–5 TECU above the real ionospheric TEC values (Jee et al. 2010; Wang et al. 2017). As a reliable TEC data source, the JASON TEC data, for high (December 2014) and low (September 2017) sunspot periods, were also used as a reference to assess the performance of the SF ionospheric TEC estimation method.

For comparison, each panel in Fig. 6 shows the JASON TEC and BDS TEC calculated using the SF and DF methods at the locations and times of the JASON satellite orbits on a randomly selected day from the large number of consistent results. It can be seen that the JASON TEC and BDS-based TEC estimates determined using both the SF and DF methods show a similar variation tendency, again showing that both the SF and DF approaches are able to reproduce the spatial and temporal variations of the local ionosphere. Using the JASON TEC as a reference, we calculated the mean bias and RMS for the SF and DF VTEC time series for the test period and present the results in Fig. 7. Note that since the JASON data for the period DOY 258–273 in 2017 and BDS SDCB data for DOY 341 and 347 in 2014 cannot be downloaded from the main IGS server, statistics for this period are not included in Fig. 7. As summarized in this figure, the mean RMS values are 4.60/4.67 TECU for December 2014 and 2.63/2.34 TECU for September 2017 for the SF/DF methods, respectively, showing that TEC estimates generated by the SF method and the DF method have a potential ability to match the JASON TEC.

Validation against differential STEC

The index of differential STEC (dSTEC), which is defined as the difference between the STEC measured at any point along a continuous phase arc and the STEC measured when the satellite is at its highest elevation seen from a given receiver (Hernández-Pajares et al. 2017), has also been used for comparing the performance of the SF method. According to the study of Feltens et al. (2011), the measured dSTEC "truth" can be directly obtained from the GF combination of the raw DF phases when no cycle slips occur over a phase continuous measurement arc, with an accuracy of less than 0.1 TECU.

Figure 8 shows the mean dSTEC errors and the RMS errors of the dSTEC for the SF and DF methods at each randomly selected receiver under different solar activity levels. It is apparent that the mean RMS values are 5.62/5.43 TECU for December 2014 and 3.35/3.02 TECU for September 2017 for the SF/DF methods, respectively, showing that there is no significant difference in the ability to capture both spatial and temporal gradients in the ionosphere between the SF and DF methods.

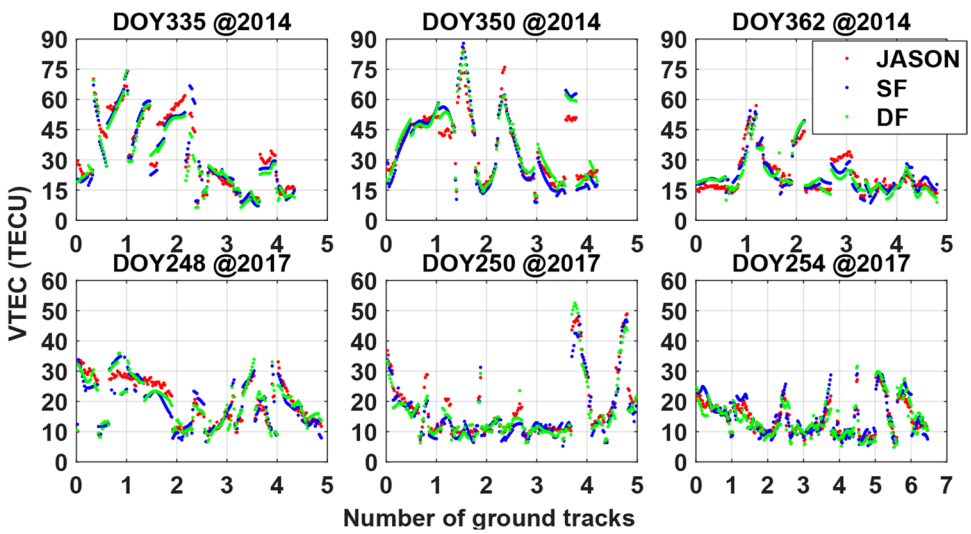

Fig. 6 VTEC estimates at each IPP from the BDS B1 + B2 data (in green), from the BDS B1 data (in blue), and from the JASON data (in red) on a day in December 2014 and September 2017. Note that the unit of "number of ground tracks" on the horizontal axis is fifty

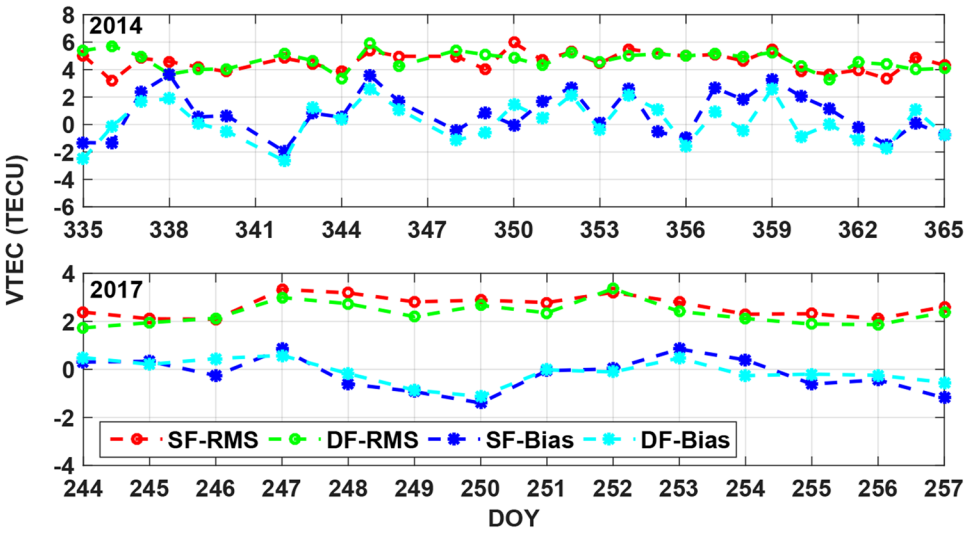

Fig. 7 Daily mean and RMS of the differences between the VTEC estimates and the JASON reference data for December 2014 and September 2017 (unit: TECU)

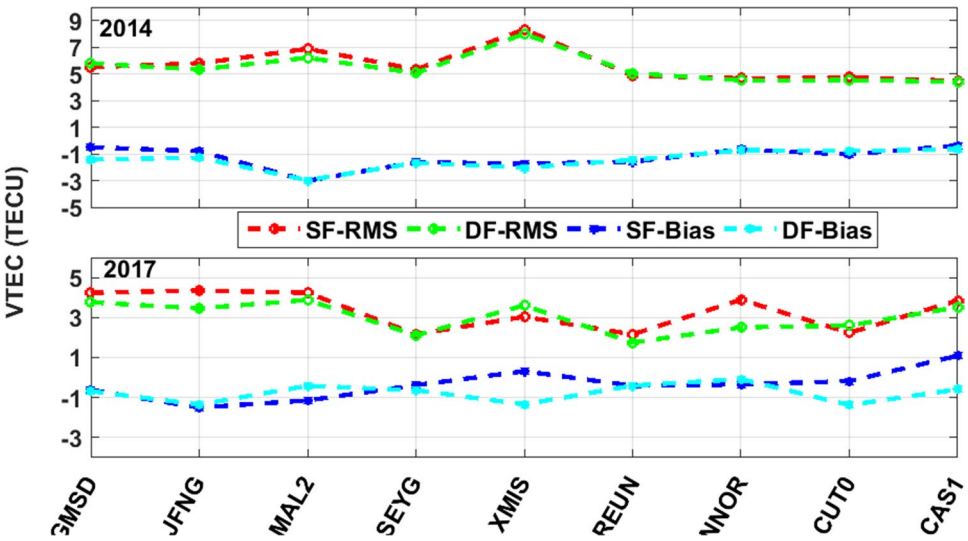

Fig. 8 Mean value of monthly dSTEC-BDS error and the RMS error of the dSTEC-BDS for the SF PPP and DF CCL

Conclusions

To eliminate the requirement of the customary dual-frequency (DF) approach for code and phase data on two frequencies, a new ionospheric total electron content (TEC) estimation procedure based on single-frequency (SF) BDS data is proposed in this study. The implementation of the proposed method consists of two procedures: first, retrieve ionospheric observables employing SF precise point positioning (PPP) instead of carrier-to-code leveling (CCL) used in the customary DF method; second, isolate the ionospheric TEC from the ionospheric observables by modeling ionospheric TEC using the adjusted spherical harmonic (ASH) expansion and introducing the a priori SDCB estimates provided by the German aerospace center (DLR) and Chinese academy of sciences (CAS).

To assess the performance of the proposed approach, the ionospheric TEC are estimated using a set of BDS measured data collected from receivers of MGEX network for a high (December 2014) and low (September 2017) sunspot period. The accuracy of ionospheric TEC estimated by both the SF and DF methods are validated by comparing them with external TEC data sources. Based on our analysis, we can conclude that the ionospheric VTEC derived using the SF method from the BDS B1 data and using the DF method from the BDS B1 + B2 data are both capable of reproducing the spatial and temporal variations of the ionosphere. Taking the TEC estimates obtained from the IGS final combined global ionospheric map (GIM) product as a reference, the mean RMS of the TEC estimates obtained from the SF approach and DF method are 5.77/6.80 TECU for December 2014 and 3.65/2.48 TECU for September 2017, respectively. The TEC estimates generated by the SF method and the DF

method have a comparable ability to match the JASON TEC, with average RMS errors at the level of 4.60/4.67 TECU for December 2014 and 2.63/2.34 TECU for September 2017, respectively. Compared to the BDS-measured differential STEC (dSTEC), the mean RMS errors determined using the SF and DF approaches are 5.62/5.43 TECU for December 2014 and 3.35/3.02 TECU for September 2017, respectively. It can be concluded that the TEC determination performances of the SF PPP and DF CCL approaches are roughly equal.

Overall, the SF approach is a promising way to monitor ionospheric TEC based on SF BDS data. Compared to the customary DF approach, the SF method is more attractive and competitive in cost and has greater potential to be popularized to the mass-market SF receivers that can support BDS code and phase data on only one frequency. It may become possible to use mass-market SF receivers to increase the spatial and temporal resolution of ionospheric information in land areas in the future.

Acknowledgements Many thanks are due to the IGS for providing access to the Multi-GNSS Experiment (MGEX) data, the ionospheric GIM products, and the differential code bias (DCB) products. This work was supported by the National Key Research Program of China "Collaborative Precision Positioning Project" (No. 2016YFB0501900) and China Natural Science Funds (41604031, 41774042 and 41621091). The second author is supported by the CAS Pioneer Hundred Talents Program. The third author is supported by LU JIAXI International team program supported by the K.C. Wong Education Foundation and CAS.

References

Brunini C, Azpilicueta FJ (2009) Accuracy assessment of the GPS-based slant total electron content. J Geod 83(8):773–785

Brunini C, Azpilicueta F (2010) GPS slant total electron content accuracy using the single layer model under different geomagnetic regions and ionospheric conditions. J Geod 84(5):293–304

Brunini C, Meza A, Bosch W (2005) Temporal and spatial variability of the bias between TOPEX-and GPS-derived total electron content. J Geod 79(4–5):175–188

Ciraolo L, Azpilicueta F, Brunini C, Meza A, Radicella S (2007) Calibration errors on experimental slant total electron content (TEC) determined with GPS. J Geod 81(2):111–120

Feltens J, Schaer S (1998) IGS Products for the Ionosphere, IGS Position Paper. In: Proceedings of the IGS analysis centers workshop, ESOC, Darmstadt, Germany, February 9–11, pp 225–232

Feltens J, Angling M, Jackson-Booth N, Jakowski N, Hoque M, Hernández-Pajares M, Aragón-Àngel A, Orús R, Zandbergen R (2011) Comparative testing of four ionospheric models driven with GPS measurements. Radio Sci 46 (RS0D2):1–11

Guo J, Xu X, Zhao Q, Liu J (2016) Precise orbit determination for quad-constellation satellites at Wuhan University: Strategy, result validation, and comparison. J Geod 90(2):143–159

Hernandez-Pajares M, Juan JM, Sanz J (1999) New approaches in global ionospheric determination using ground GPS data. J Atmos Sol Terr Phys 61(16):1237–1247

Hernandez-Pajares M, Miguel Juan J, Sanz J, Aragon-Angel A, Garcia-Rigo A, Salazar D, Escudero M (2011) The ionosphere: effects, GPS modeling and the benefits for space geodetic techniques. J Geod 85(12):887–907

Hernández-Pajares M, Juan JM, Sanz J, Orus R, Garcia-Rigo A, Feltens J, Komjathy A, Schaer SC, Krankowski A (2009) The IGS VTEC maps: a reliable source of ionospheric information since 1998. J Geod 83(3–4):263–275

Hernández-Pajares M, Roma-Dollase D, Krankowski A, García-Rigo A, Orús-Pérez R (2017) Methodology and consistency of slant and vertical assessments for ionospheric electron content models. J Geod 91(12):1405–1414

Jee G, Lee HB, Kim YH, Chung JK, Cho J (2010) Assessment of GPS global ionosphere maps (GIM) by comparison between CODE GIM and TOPEX/Jason TEC data: Ionospheric perspective. J Geophys Res Space Phys 115(A10319):1–11

Komjathy A, Sparks L, Wilson BD, Mannucci AJ (2005) Automated daily processing of more than 1000 ground-based GPS receivers for studying intense ionospheric storms. Radio Sci 40(RS6006):1–7

Krankowski A, Kosek W, Baran L, Popinski W (2005) Wavelet analysis and forecasting of VTEC obtained with GPS observations over European latitudes. J Atmos Sol Terr Phy 67(12):1147–1156

Leick A, Rapoport L, Tatarnikov D (2015) GPS satellite surveying, 4th edn. Wiley, New York

Li W, Cheng P, Bei J, Wen H, Wang H (2012) Calibration of regional ionospheric delay with uncombined precise point positioning and accuracy assessment. J Earth Syst Sci 121(4):989–999

Li M, Yuan YB, Wang NB, Li ZS, Li Y, Huo XL (2017a) Estimation and analysis of Galileo differential code biases. J Geod 91(3):279–293

Li W, Nadarajah N, Teunissen PJG, Khodabandeh A, Chai YJ (2017b) Array-Aided Single-Frequency State-Space RTK with Combined GPS, Galileo, IRNSS, and QZSS L5/E5a Observations. J Surv Eng 143(4):04017006

Li M, Yuan Y, Zhang B, Wang N, Li Z, Liu X, Zhang X (2018a) Determination of the optimized single-layer ionospheric height for electron content measurements over China. J Geod 92(2):169–183

Li M, Yuan Y, Wang N, Liu T, Chen Y (2018b) Estimation and analysis of the short-term variations of multi-GNSS receiver differential code biases using global ionosphere maps. J Geod 92(8):889–903

Liu T, Yuan Y, Zhang B, Wang N, Tan B, Chen Y (2016) Multi-GNSS precise point positioning (MGPPP) using raw observations. J Geod 91(3):253–268

Liu T, Zhang B, Yuan Y, Li M (2018) Real-Time Precise Point Positioning (RTPPP) with raw observations and its application in real-time regional ionospheric VTEC modeling. J Geod 92(11):1267–1283

Mannucci AJ, Wilson BD, Yuan DN, Ho CH, Lindqwister UJ, Runge TF (1998) A global mapping technique for GPS-derived ionospheric total electron content measurements. Radio Sci 33(3):565–582

Montenbruck O, Steigenberger P (2013) The BeiDou navigation message. J Glob Position Syst 12(1):1–12

Montenbruck O, Hauschild A, Steigenberger P (2014) Differential code bias estimation using Multi-GNSS observations and global ionosphere maps. Navigation 61(3):191–201

Odijk D, Zhang B, Khodabandeh A, Odolinski R, Teunissen PJ (2016) On the estimability of parameters in undifferenced, uncombined GNSS network and PPP-RTK user models by means of S-system theory. J Geod 90(1):15–44

Orus R, Cander LR, Hernandez-Pajares M (2007) Testing regional vertical total electron content maps over Europe during the 17–21 January 2005 sudden space weather event. Radio Sci 42(RS3002):1–12

Schaer S (1999) Mapping and Predicting the Earth's Ionosphere Using the Global Positioning System. Doctoral dissertation, Univ. Bern, Switzerland

Schueler T, Oladipo OA (2014) Single-frequency single-site VTEC retrieval using the NeQuick2 ray tracer for obliquity factor determination. GPS Solut 18(1):115–122
Schueler T, Oladipo OA (2013) Single-frequency GNSS retrieval of vertical total electron content (VTEC) with GPS L1 and Galileo E5 measurements. J Space Weather Space Clim 3:(A11)
Shu B, Liu H, Xu L, Gong X, Qian C, Zhang M, Zhang R (2016) Analysis of satellite-induced factors affecting the accuracy of the BDS satellite differential code bias. GPS Sol 21(3):905–916
Wang N, Yuan Y, Li Z, Huo X (2016a) Improvement of Klobuchar model for GNSS single-frequency ionospheric delay corrections. Adv Space Res 57(7):1555–1569
Wang N, Yuan Y, Li Z, Montenbruck O, Tan B (2016b) Determination of differential code biases with multi-GNSS observations. J Geod 90(3):209–228
Wang N, Yuan Y, Li Z, Li Y, Huo X, Li M (2017) An examination of the Galileo NeQuick model: comparison with GPS and JASON TEC. GPS Solut 21(2):605–615
Wu S, Peck S, Schempp T, Shloss P, Wan H, Buckner P, Doherty P, Angus J (2006) A single frequency approach to mitigation of ionospheric depletion events for SBAS in equatorial regions. In: Proc. ION GNSS 2006, Institute of Navigation, Fort Worth, Texas USA, September 26–29, pp 939–952
Yuan Y, Ou J (2001) An improvement to ionospheric delay correction for single-frequency GPS users—the APR-I scheme. J Geod 75(5–6):331–336
Yuan Y, Li Z, Wang N, Zhang B, Li H, Li M, Huo X, Ou J (2015) Monitoring the ionosphere based on the Crustal Movement Observation Network of China. Geodesy Geodyn 6(2):73–80
Zhang B (2016) Three methods to retrieve slant total electron content measurements from ground-based GPS receivers and performance assessment. Radio Sci 51(7):972–988
Zhang BC, Ou JK, Yuan YB, Li ZS (2012) Extraction of line-of-sight ionospheric observables from GPS data using precise point positioning. Sci China-Earth Sci 55(11):1919–1928
Zhang B, Teunissen PJG, Yuan Y, Zhang H, Li M (2017) Joint estimation of vertical total electron content (VTEC) and satellite differential code biases (SDCBs) using low-cost receivers. J Geod 92(4):401–413

Min Li is an assistant researcher at the Institute of Geodesy and Geophysics (IGG), Chinese Academy of Sciences (CAS). She received her Ph.D. degree in 2018 at IGG, CAS. Her current research interests include post and real-time GNSS ionospheric TEC modeling, determination of multi-GNSS differential code biases (DCBs), and space weather

Baocheng Zhang is a researcher at the Institute of Geodesy and Geophysics, Chinese Academy of Sciences in Wuhan. His research is focused on multi-GNSS integer ambiguity resolution enabled precise point positioning (PPP-RTK), with an emphasis on code and carrier phase bias estimation and characterization, ionospheric delay retrieval and prototype PPP RTK network software development

Yunbin Yuan is a researcher and the director of GNSS Application and Research Group, Institute of Geodesy and Geophysics, Chinese Academy of Sciences. His current research interests are the following: (1) GNSS-based spatial environmental monitoring and analysis; (2) high-precision GNSS satellite navigation and positioning; (3) GNSS in orbit-determination applications; (4) system imitation test

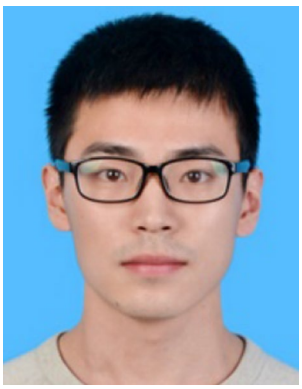

Chuanbao Zhao received his B.S. in Surveying and Mapping Engineering from Hefei University of Technology, Hefei, China in 2015. He is currently working toward his Ph.D. degree in Geodesy in the Institute of Geodesy and Geophysics, Chinese Academy of Sciences, Wuhan, China. His current research focuses on multi-GNSS precise point positioning algorithms and related applications